Contents lists available at ScienceDirect

Applied Catalysis B: Environmental

A feasibility study of niobium-containing materials for oxygen storage in three way catalytic converters

A. Simson, K. Roark, R. Farrauto *

Department of Earth and Environmental Engineering, Columbia University, United States

A B S T R A C T

Materials containing Ce–Zr–Y and doped with between 0 and 15% niobium were analyzed for their oxygen storage capacity as potential materials for use in the three-way catalyst (TWC). An optimum amount of niobium was identified (7.5 cat mol%) that led to significantly higher oxygen storage capacity than the baseline niobium-free sample ($Zr_{0.70}Ce_{0.22}Y_{0.08}O_x$) at temperatures within the typical operating range of the TWC. The niobium-containing material also had higher rates and extents of reduction and oxidation than the baseline material during redox cycling tests performed at 500 °C. In addition to niobium as a potential dopant, Ce–Zr–Y formulations containing either Nd or Pr were also analyzed and the order of performance was found to be: Nb > Nd > Pr. Characterization of all niobium-containing materials indicated that niobium integrated into the Ce–Zr–Y oxide phase. In the future, the niobium-containing materials will be compared to state-of-the-art OSC materials in redox cycling environments more typical of the TWC.

© 2014 Elsevier B.V. All rights reserved.

1. Introduction

The purpose of the three-way catalyst (TWC) in gasoline vehicles is to achieve high conversion of carbon monoxide, unburned hydrocarbons and NO_x pollutants produced in the internal combustion engine. Their high conversion is ensured by maintaining a narrow air/fuel ratio (near $\lambda = 1$, stoichiometric) in the exhaust using an oxygen storage component (OSC) in the catalyst coupled with an electronic feedback control system. OSC materials have facile redox properties and thus can readily supply oxygen when the reaction is operating fuel rich ($\lambda < 1$) and remove oxygen when the reaction is operating fuel lean ($\lambda > 1$). For example, the reactions below demonstrate how ceria can contribute to oxygen storage in the TWC:

$$Reduction(\lambda < 1, insufficient O_2): 2CeO_2 + CO \rightarrow Ce_2O_3 + CO_2$$

$$Oxidation(\lambda > 1, excess O_2): Ce_2O_3 + O_2 \rightarrow 2CeO_2$$

Pure ceria, with facile CeO_2/Ce_2O_3 redox capacity, was the primary oxygen storage component in the TWC until it was found that CeO_2–ZrO_2 solid solutions had better performance [1–3]. Since

then, CeO_2–ZrO_2 solid solutions, frequently containing additional dopants such as Y, have been commercialized for use in the TWC.

Dopants to either pure ceria or ceria–zirconia solutions have been investigated to determine whether they can increase the total oxygen storage capacity, increase the reduction and oxidation rates, or improve the thermal stability of the OSC. The most effective dopants have typically been trivalent rare earth cations, such as La [4–9], Y [4–7,9–11], Pr [6,9,12–14], Ga [4], or Nd [4,6,9,12,14]. Studies have also investigated alkali-earth metals such as Ca [15,16], Mg [16], Sr [19–21], and Ba [21], transition metals such as Mn [17,18], Fe [22], and Co [22,14], or other elements including Sm [5], Bi [14], and Al [23]. The use of niobium in ceria–zirconia oxides was suggested in a 2003 patent by Delphi [15], which showed a promising impact of niobium on the OSC, but the use of niobium has not been further reported for this application.

Within the last few years the family of rare earths, including cerium, experienced a rapid increase in price upsetting the markets and initiating a search for methods to reduce their concentrations in the OSC. Similar to many of the effective rare earth dopants, niobium has a small ionic radius and is similar in size to zirconia. However, niobium pentoxide has thermodynamically poor redox properties in the operating range of the OSC (300–600 °C). Despite this, the Delphi's patent reports that niobium can enhance the oxygen storage capacity of Ce-containing materials [15]. Thus, the goal of this feasibility study is to determine whether niobium can enhance the oxygen storage capacity of the Ce-containing OSC, which could allow a decrease in the amount of cerium and other

* Corresponding author at: Department of Earth and Environmental Engineering, Columbia University in the City of New York, 500W. 120th Street, New York, NY 10027, United States. Tel.: +1 212 854 6390; fax: +1 732 438 1090.
E-mail address: rf2182@columbia.edu (R. Farrauto).

rare earth elements that are present. It is understood that testing in a TWC exhaust would be a required step in advancing this new material for real applications.

2. Experimental

2.1. Catalyst preparation

To determine the impact of niobium on common OSC formulations, oxides containing a constant ratio of Ce, Zr, and Y with increasing amounts of Nb were synthesized and assessed for their oxygen storage capacity. To prepare the materials, a water solution of the precursors, $Ce(NO_3)_3$, $ZrO(NO_3)_2$, $Y(NO_3)_3$, and ammonium niobate (V) oxalate ($C_6H_4NNbO_{12}$), was added by buret to vigorously stirred 0.2 M solution of ammonium hydroxide. Following precipitation, samples were filtered, triple washed, dried, and calcined (for 2 h in air at 550 °C). Samples were aged at 800, 900, or 1000 °C for 2 h in air. Niobium pentoxide (Nb_2O_5), used as a baseline, and the ammonium niobate (V) oxalate, used as a precursor, were graciously provided by CBMM (Compendio Brasileiro de Metalurgia e Mineracao).

As a baseline comparison to the niobium-containing samples, both a niobium-free sample containing Ce, Zr, and Y ($Nb0 = Zr_{0.70}Ce_{0.22}Y_{.08}O_x$) and a pure ceria–zirconia ($Zr_{0.76}Ce_{0.24}O_x$) were studied. All samples had the same Zr:Ce ratio as niobium-containing samples (3.25) and the preparation procedures were the same as those stated above excluding the addition of relevant precursors. The yttrium-containing baseline sample outperformed the pure ceria–zirconia sample for every condition studied and is therefore used as the primary baseline material throughout the paper. Additionally, to test the impact of preparation method, a niobium-impregnated sample was prepared using the incipient wetness method. For this sample the baseline niobium-free sample ($Nb0 = Zr_{0.70}Ce_{0.22}Y_{.08}O_x$) was calcined at 550 °C for 2 h in air and then impregnated with the niobium oxalate to obtain the same Nb:Ce:Zr:Y ratio as the Nb2 sample in Table 1 (7.5 cation wt% Nb). The sample was then re-calcined for 2 h in air at 550 °C and aged. Samples impregnated with precious metal were prepared using the incipient wetness method with the pre-calcined OSC materials (550 °C) and a non-alkali, non-chloride platinum precursor. Samples were impregnated to achieve a loading of 0.5 wt% Pt and were re-calcined (for 2 h in air at 550 °C) and aged.

2.2. Performance testing and characterization

A measurement related to the oxygen storage capacity of each material was assessed using thermal gravimetric analysis (TGA) using a Netzsch STA 449F3 unit. Temperature programmed reduction and oxidation (TPR/TPO) measurements were performed with a heating and cooling rate of 5 °C/min. Samples were dried in nitrogen at 150 °C for 1 h in the TGA prior to all measurements. For TPR segments, samples were heated in 100 mL/min of 2% H_2/N_2; for TPO segments, samples were exposed to the same heating rates in 120 mL/min of 1% O_2/N_2. In addition to TPR/TPO testing, isothermal redox cycling was performed at 500 °C. Ten cycles alternating between 60-min reducing segments (2% H_2/N_2) and 60-min oxidizing segments (1% O_2/N_2) were performed. Both the TPR/TPO tests and redox cycling tests were repeated on additional preparations of each formulation for reproducibility.

Materials were characterized using BET, XRD and Raman and niobium concentrations in selected samples were verified using XRF. Single-point BET surface area was collected using a Quantachrome ChemBET. Room temperature XRD was performed to provide insight into the structure of the samples and the solubility of niobium into the oxide solutions. Powder XRD patterns
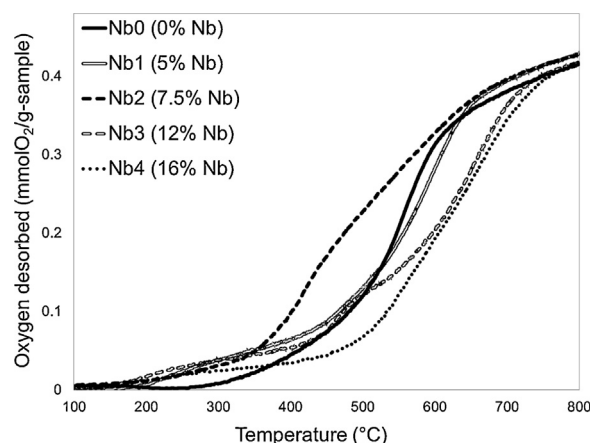

Fig. 1. Total oxygen desorbed by each material in Table 1 during TPR (5 °C/min in 100 mL/min of 2% H_2/N_2) after aging at 800 °C for 2 h in air.

were recorded with an X'Pert Pro PANalytical X-ray diffractometer using Cu-Kα radiation of wavelength 1.541 Å, a scanned angle range 10°–100° with step size of 0.01° and count time per step of 60 s. Raman spectra were collected using a LabRam Aramis microscope (Horiba) equipped with a 500-mW 532-nm laser as the excitation source. The beam was attenuated with a D1 filter. Spectra were collected using a 1200 grooves/mm diffraction grating and a 50× objective lens. XRF was completed on a Bruker S4 wavelength dispersive spectrometer to confirm the niobium concentrations in selected samples.

3. Results

3.1. Oxygen storage capacity of niobium-containing materials

The primary materials investigated were Ce–Zr–Y oxides with varying amounts of niobium. The composition of these materials, including their cerium and niobium concentrations (cation mole%), and their BET surface areas after aging for 2 h in air at 800, 900, or 1000 °C are given in Table 1. These aging temperatures represent the upper limit of temperatures expected in the automobile exhaust. Increasing niobium concentrations led to lower BET surface areas but all materials (including the niobium-free material) had significant losses in surface area after aging at 900 or 1000 °C.

A model test for oxygen storage capacity of each material was performed by measuring the oxygen released by the material during reduction cycles (as a weight loss) or by measuring the oxygen consumed by the material during oxidation cycles (as a weight gain). It should be mentioned that oxidation is relatively fast compared to the reduction so only the reduction will be used to assess the assumed oxygen storage capacity of the materials. The total oxygen released by the material during the first reduction cycle (measured as a weight loss and translated into mmol O_2/g sample) for each material is shown in Fig. 1. From this data, the total oxygen released by each material at 500, 400 and 300 °C is plotted as a function of niobium concentration in Fig. 2. The data in these figures represent the average of at least two separately prepared samples of each formulation. The maximum error in the reduction capacity (mmol O_2/g sample) at any given temperature never exceeded 8% for samples of the same formulation.

As shown in Figs. 1 and 2, all formulations containing niobium had higher oxygen storage capacity than the baseline Nb0 material ($Zr_{0.70}Ce_{0.22}Y_{0.08}O_x$) between 150 and 350 °C. In addition to the enhancement in reduction that was measured between 150 and 350 °C for all niobium-containing samples, the Nb2 sample ($Zr_{0.65}Ce_{0.20}Y_{0.075}Nb_{0.075}O_x$) exhibited enhanced reduction

Table 1
Formulations tested and associated BET surface area after aging at 800, 900 or 1000 °C for 2 h in air.

Name	Formula	% Ce (cat mol%)	% Nb (cat mol%)	S_{BET} 800 °C [m² g⁻¹]	S_{BET} 900 °C [m² g⁻¹]	S_{BET} 1000 °C [m² g⁻¹]
Nb0	$Zr_{0.70}Ce_{0.22}Y_{0.08}O_x$	22	0	40.4	20.5	6.3
Nb1	$Zr_{0.67}Ce_{0.21}Y_{0.077}Nb_{0.05}O_x$	21	5	30.1	18.9	3.9
Nb2	$Zr_{0.65}Ce_{0.20}Y_{0.75}Nb_{0.075}O_x$	20	7.5	27.0	16.4	3.1
Nb3	$Zr_{0.61}Ce_{0.19}Y_{0.071}Nb_{0.12}O_x$	19	12	26.3	12.3	<1
Nb4	$Zr_{0.59}Ce_{0.18}Y_{0.068}Nb_{0.16}O_x$	18	16	25.7	11.4	<1
Nb2noY	$Zr_{0.70}Ce_{0.22}Nb_{0.08}O_x$	22	8	29.9	11.0	<1

between 350 and 600 °C. At 500 °C, the Nb2 sample desorbed almost twice the amount of oxygen as the niobium-free baseline material. The enhanced reduction in this temperature range correlates well with the operating range of the TWC. Further, Nb2 outperformed the baseline for the entire range of temperatures investigated. Above 600 °C, both the Nb2 and Nb1 ($Zr_{0.67}Ce_{0.21}Y_{0.077}Nb_{0.05}O_x$) samples desorbed more oxygen than the baseline. By 800 °C, all samples had similar extents of reduction per gram material (within 2.5%). However, due to the lower ceria concentrations in the niobium-containing samples (from the dilution effect of niobium), these samples demonstrated even higher oxygen storage capacity per gram cerium than the values represented in Figs. 1 and 2. Assuming the initial stoichiometry of oxygen in each formulation is $x = 2$, the total oxygen desorbed by each sample (by 800 °C) can be converted to a percent of the theoretically expected value based on a Ce +4/+3 transition. This value was greater than 100% for all niobium-containing samples and increased linearly with niobium concentration to an ultimate value of 120% for the highest niobium-containing sample (Nb4 = $Zr_{0.59}Ce_{0.18}Y_{0.068}Nb_{0.16}O_x$). The additional extent of reduction measured at 800 °C may be due to the reduction of niobium at these high temperatures. The greater extents of reduction at lower temperatures with the niobium may be due to an impact of niobium on the structure of the ceria, which increases oxygen diffusion rates. We could also speculate that by incorporating Nb (+5) into a Ce (+4) structure we are creating an oxygen deficiency. The structure will therefore need a negative O species which can enhance O transfer. This is the opposite analogy for zeolite acidity when an Al (+3) is incorporated into the Si (+4) tetrahedral and requires a proton for charge balance.

3.2. Effect of preparation methods, dopants, and precious metal addition

The results in Figs. 1 and 2 demonstrate that the addition of niobium to traditional Ce–Zr–Y oxides can increase their oxygen storage capacity within the operating range of the TWC. However, niobium in its pentoxide state does not begin to reduce
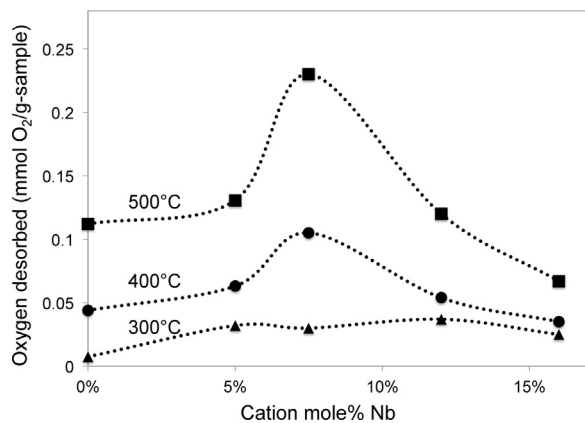
until approximately 650 °C and only reduces to a limited extent within the temperature range studied. Therefore, an isolated phase of Nb_2O_5 is not expected to contribute to the enhanced oxygen storage capacity demonstrated for the Nb2 sample. In order to further demonstrate this, a Ce–Zr–Y oxide was impregnated with the niobium precursor so the resultant sample had equivalent concentrations of Ce, Zr, Y and Nb to the Nb2 sample. The reduction profiles of the two different formulations of Nb2; one prepared by co-precipitation and one prepared by impregnation of the niobium onto the Ce–Zr–Y oxide after calcination; are compared in Fig. 3. It was found that only the co-precipitated sample led to an enhancement in reduction below 600 °C. Thus, to have an effect the niobium must be co-precipitated with the other precursors to create a solid solution. As discussed in Section 3.4, characterization of these niobium-containing materials (by XRD and Raman) has further indicated that the niobium in the co-precipitated samples was integrated into the Ce–Zr–Y oxide phase.

The highest performing sample in Figs. 1 and 2, Nb2 ($Zr_{0.65}Ce_{0.20}Y_{0.075}Nb_{0.075}O_x$), had equivalent concentrations of yttrium and niobium. Previous work on similar materials also found that this formulation, with equivalent amounts of yttrium and niobium, was the most optimum for oxygen storage capacity [15]. In order to determine whether the yttrium contributed to the enhanced oxygen storage of these materials, a formulation of Nb2 was prepared without the yttrium (Nb2noY: $Zr_{0.70}Ce_{0.22}Nb_{.08}O_x$). As shown in Fig. 4, the yttrium-containing sample had slightly higher performance than the yttrium-free sample; however, both samples had similar profiles compared to the baseline, niobium-free material. These results indicate that the enhancement of oxygen storage performance that is observed, particularly with the Nb2 sample, is a result of primarily the niobium concentration and that the yttrium is not necessary to achieve a benefit in oxygen storage capacity. It should be stated that the sample that did not contain yttrium had a lower surface area compared to the standard Nb2 after aging at 800 °C and a higher Ce concentration (Table 1).
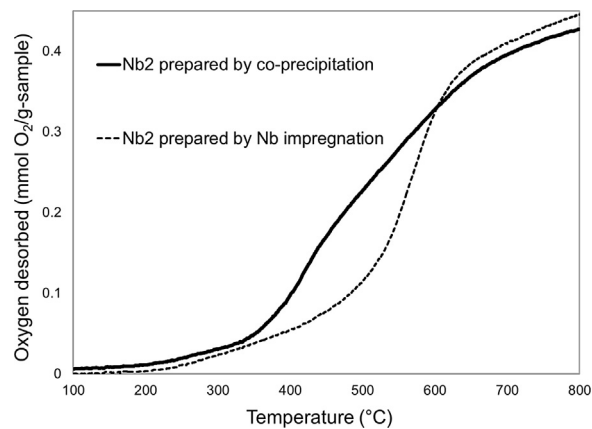

Fig. 2. Total oxygen desorbed by each material at 300, 400 or 500 °C plotted as a function of each material's Nb concentration.

Fig. 3. Total oxygen desorbed during TPR (5 °C/min in 100 mL/min of 2% H_2/N_2) for Nb2 prepared by either coprecipitation ($Zr_{0.65}Ce_{0.20}Y_{0.075}Nb_{0.075}O_x$) or by impregnation of niobium: Nb/Nb0 ($Nb_{0.075}/Zr_{0.65}Ce_{0.20}Y_{0.075}O_x$). All samples aged at 800 °C for 2 h in air.
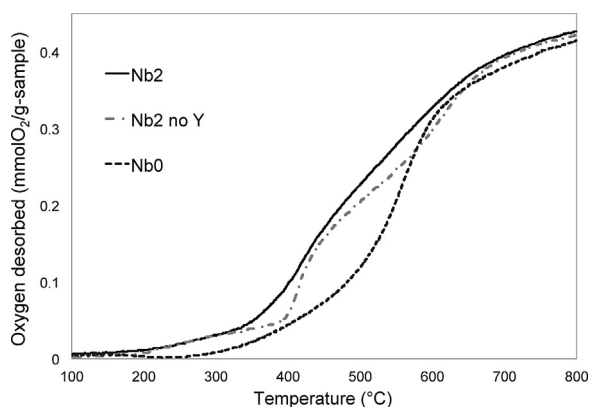
Fig. 4. Total oxygen desorbed during TPR ($5\,^\circ$C/min in 100 mL/min of 2% H_2/N_2 flow) for the Nb2 ($Zr_{0.65}Ce_{0.20}Nb_{.075}Y_{.075}O_x$) and Nb2-noY sample ($Zr_{0.70}Ce_{0.22}Nb_{.08}O_x$), and baseline Nb0 ($Zr_{0.70}Ce_{0.22}Y_{.08}O_x$). All samples aged at $800\,^\circ$C for 2 h in air.

In addition to yttrium, many other dopants, particularly rare earth dopants such as praseodymium and neodymium have been used in OSC formulations to improve the overall oxygen storage capacity of ceria–zirconia materials. Thus, in order to study the potential for niobium as a dopant to the OSC, the highest performing niobium sample (Nb2 = $Zr_{0.65}Ce_{0.20}Nb_{.075}Y_{.075}O_x$,) was compared to formulations containing the same amount of Ce, Zr, and Y with either praseodymium ($Zr_{0.65}Ce_{0.20}Pr_{.075}Y_{.075}O_x$) or neodymium ($Zr_{0.65}Ce_{0.20}Nd_{.075}Y_{.075}O_x$) as a substitute for the niobium. The temperature programmed reduction profiles for these materials are compared in Fig. 5. The niobium-containing sample outperformed the other materials for the full range of temperatures studied. The order of performance of the samples was: Nb > Nd > Pr. Additionally, the total oxygen desorbed by $800\,^\circ$C was higher for the niobium-containing samples than for the materials containing the other dopants.

In order to more closely replicate a material used in an actual OSC, the materials were impregnated with precious metal. The materials from Table 1 were calcined and impregnated with Pt to achieve a 0.5 wt% Pt loading. Temperature programmed reduction profiles for these samples performed after aging at $800\,^\circ$C are shown in Fig. 6. As expected, Pt increased the extent of reduction at low temperatures for all samples. However, the niobium-containing materials reduced more rapidly than the niobium-free sample for the Nb1, Nb2 and Nb3 sample (Nb4 sample not shown). Similar to the TPR results in Section 3.1, the Pt-impregnated Nb2 had the greatest extent of reduction below $500\,^\circ$C. These results indicate that niobium-containing Ce–Zr oxides may be applicable
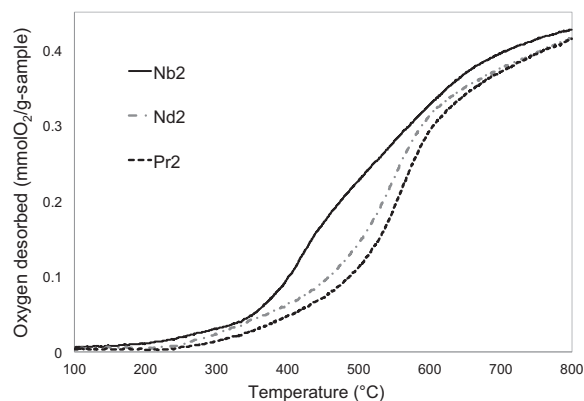

Fig. 5. Total oxygen desorbed during TPR ($5\,^\circ$C/min in 100 mL/min of 2% H_2/N_2 flow) for the Nb2 ($Zr_{0.65}Ce_{0.20}Nb_{.075}Y_{.075}O_x$), Nd2 ($Zr_{0.65}Ce_{0.20}Nd_{.075}Y_{.075}O_x$), and Pr2 ($Zr_{0.65}Ce_{0.20}Pr_{.075}Y_{.075}O_x$). All samples aged at $800\,^\circ$C for 2 h in air.
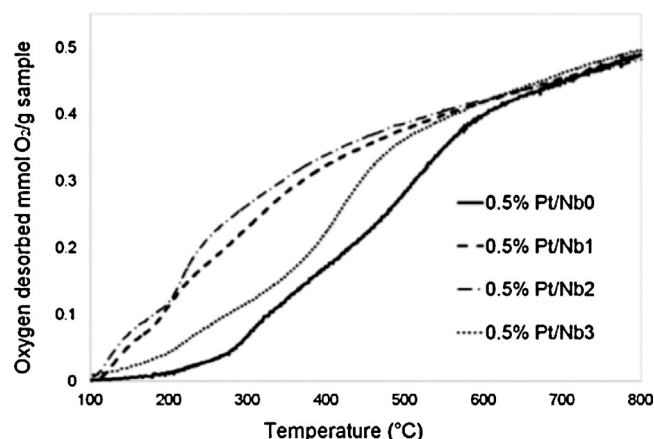

Fig. 6. Total oxygen desorbed by the materials in Table 1 with the addition of 0.5% Pt during TPR ($5\,^\circ$C/min in 100 mL/min of 2% H_2/N_2) after aging at $800\,^\circ$C for 2 h in air.

for use in the TWC. Future work will compare the Nb-containing samples to commercial OSC materials and will utilize aging conditions more typical of automobile exhaust to better understand the potential of these materials.

3.3. Rates of reduction and oxidation

Preliminary investigations of the rates of oxidation and reduction of these materials have demonstrated that niobium can increase the rate of reduction and oxidation within the operating temperature range of the TWC. Ten redox cycles were performed at $500\,^\circ$C on the Nb0 and Nb2 samples and the 1st and 10th cycles of reduction and oxidation are shown in Fig. 7a–d. For all cycles the niobium-containing sample maintained a faster rate of reduction and rate of oxidation than the baseline sample. The redox cycling improved the extents and rates during both reduction and oxidation segments for both samples. This result is consistent with several papers that have reported an increase in oxygen storage capacity of Ce–Zr and Ce–Zr–Y oxides after redox cycling [16–18]. The rate of reduction for the Nb2 sample during the 10th cycle was 0.027 mmol O_2/g-min, whereas the rate of reduction for the Nb0 sample during this cycle was 0.016 mmol O_2/g-min. The oxidation rates for the two materials were comparable. Further, after 10 cycles at $500\,^\circ$C, the Nb2 sample maintained the enhancement in reduction rate over the Nb0 sample demonstrating its durability. At $500\,^\circ$C CeO_2 is expected to release oxygen solely from the surface; however, CeO_2–ZrO_2 solid solutions are expected to release oxygen from both the surface and the bulk [3]. Similar to zirconium, niobium may further increase the oxygen diffusion rates through the bulk allowing for additional reduction at this temperature..

3.4. Characterization of materials

Room temperature XRD was performed to provide insight into the structure of the samples and the reactivity of niobium ions into the Ce–Zr–Y oxide structure. The Nb0 and Nb2 samples described in Table 1 and a sample of Nb_2O_5 were characterized using XRD. Each sample had been aged in air at $800\,^\circ$C for 2 h. The diffraction patterns for these samples are shown in Fig. 8. Niobium pentoxide (Nb_2O_5) crystallites were not detectable in the Nb2 diffraction pattern, nor were they identifiable in the pattern for higher niobium-containing samples (not shown). Thus, XRD results indicated that either the niobium was fully integrated into the Ce–Zr–Y oxide or Nb_2O_5 crystallites were too small to be detected. However, Nb2 samples aged at $1000\,^\circ$C (not shown), which would have larger crystallites due to sintering, also did not have detectable
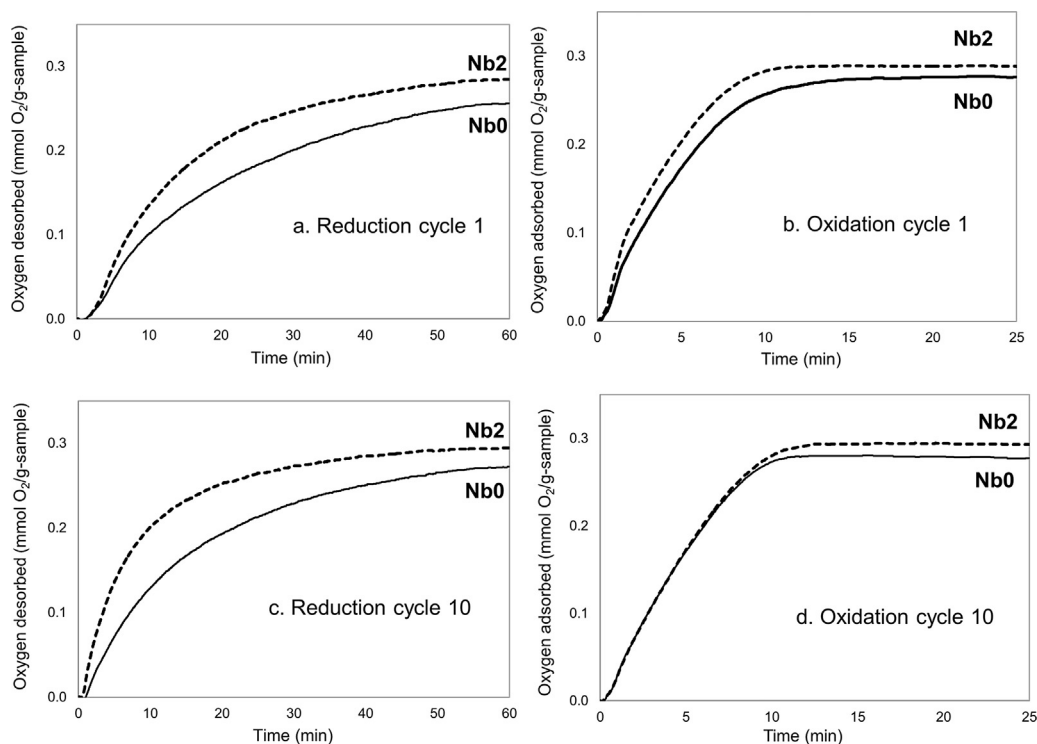
Fig. 7. Oxygen desorbed (a and c) or adsorbed (b and d) from the OSC during redox cycles performed at 500 °C with either 1% O_2/N_2 or 2% H_2/N_2 at constant flow rate of 100 mL/min.

Nb_2O_5. Thus, XRD results suggest that the niobium was incorporated into the Ce–Zr–Y oxide. Future XRD work may systematically study the impact of niobium on lattice structure.

Raman results were used to further confirm that Nb was incorporated into the Ce–Zr–Y structure and that an isolated Nb_2O_5 phase was not identifiable. The spectra for the samples described in Table 1 after aging (800 °C for 2 h in air) are shown in Fig. 9. The shifts at approximately 140, 229, 325, 469, 556, and 617 cm^{-1} identified in the baseline Nb0 sample were consistent with tetragonal Ce–Zr, Ce–Zr–Y, and Zr–Y oxide materials reported by other authors [19–22]. Peaks associated with the amorphous and crystalline form of Nb_2O_5 were not detectable. However, the shift at 770 cm^{-1} was identified for niobium-containing samples and increased in relative size with increasing niobium concentrations. This peak has been identified as Nb–O by authors who reported Raman data for Zr–Y–Nb [14]. This band was also

identified, with no frequency shift, in a Y-free Nb2 formulation (not shown). However, as shown in Fig. 9, this band was not detected in the niobium-impregnated sample, indicating that it is not likely caused by surface Nb_2O_5. Increasing concentrations of niobium (from 0 to 16 cat mol%) did not cause a continuous shift in Raman modes, consistent with an increase or decrease in lattice size, but rather caused a shift in the 260 and 640 cm^{-1} modes to higher wave numbers and a shift in the 469, and 325 cm^{-1} modes to lower wave numbers. These shifts were not observable in the niobium-impregnated sample.

The Raman spectra agree with XRD results that suggest Nb has incorporated into the Ce–Zr–Y oxide lattice. Further, Raman results suggest that Nb is affecting the structure of the CeO_2–ZrO_2 and indicates that the local bonding environment of oxygen is different. Thus far, neither the Raman results nor the XRD results indicate
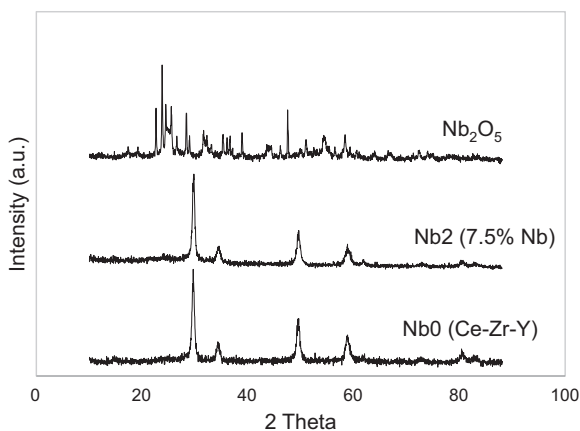

Fig. 8. XRD patterns of Nb_2O_5, Nb2 ($Zr_{0.65}Ce_{0.20}Y_{0.075}Nb_{0.075}O_x$), and Nb0 ($Zr_{0.70}Ce_{0.22}Y_{0.08}O_x$) after treatment in air at 800 °C for 2 h.
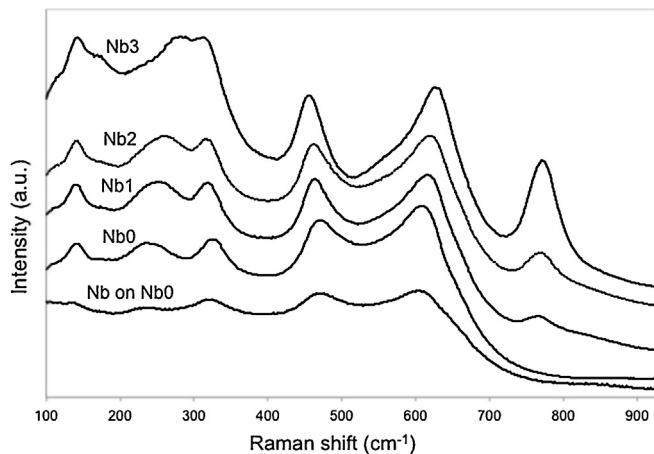

Fig. 9. Raman spectra for samples detailed in Table 1 and an Nb2 sample prepared by impregnation: Nb/Nb0 ($Nb_{0.075}/Zr_{0.65}Ce_{0.20}Y_{0.075}O_x$). All samples aged at 900 °C for 2 h in air.

why there is enhanced reduction for all niobium-containing materials at low temperature, or why there is an optimum niobium concentration (7.5 cat mol%) for reduction between 350 and 600 °C.

4. Conclusions

In this work, niobium-containing materials demonstrated high oxygen storage capacity relative to a baseline Ce–Zr–Y OSC material in the operating temperature range of the TWC. These results substantiate disclosures in a US patent by Delphi [15] while adding more fundamental data related to aging, optimization of Nb content and the material structure that gives optimum performance. An optimum amount of niobium was identified within the set of formulations studied (7.5 cat mol%). This material had greater extents of reduction than both the baseline sample ($Zr_{0.70}Ce_{0.22}Y_{0.08}O_x$) and than similar formulations containing common rare earth dopants to the OSC. Further, this material had higher rates and extents of reduction and oxidation than the baseline niobium-free material during redox cycling tests performed at 500 °C. Characterization of niobium-containing materials by XRD and Raman indicated that niobium integrated into the Ce–Zr–Y oxide phase. The addition of Pt to Nb-containing samples shows an enhancement of reduction relative to Pt additions to Nb free materials. Future work will explore the impact of niobium on the crystal structure of ceria–zirconia and other mixed oxides to understand how it contributes to increased oxygen adsorption and desorption. A comparison of the niobium-containing materials to state-of-the-art OSC materials, using redox cycling environments more typical of the TWC, will also be conducted.

Acknowledgements

References

[1] M. Sugiura, Catal. Surv. Asia 7 (2003) 77.
[2] A. Name, B. Name, C. Name, Journal Title 35 (2000) 3523.
[3] P. Fornasiero, G. Balducci, R. Di Monte, J. Kašpar, V. Sergo, G. Gubitosa, A. Ferrero, M. Graziani, J. Catal. 164 (1996) 173.
[4] A. Trovarelli, Catalysis by Ceria and Related Materials, Imperial College Press, 2002.
[5] P. Vidmar, P. Fornasiero, J. Kašpar, G. Gubitosa, M. Graziani, J. Catal. 171 (1997) 160.
[6] L.N. Ikryannikova, A.A. Aksenov, G.L. Markaryan, G.P. Murav'eva, B.G. Kostyuk, A.N. Kharlanov, E.V. Lunina, Appl. Catal. A: Gen. 210 (2001) 225.
[7] B. Zhao, Q. Wang, G. Li, R. Zhou, J. Environ. Chem. Eng. 1 (2013) 534.
[8] G. Jiaxiu, S. Zhonghua, W. Dongdong, Y. Huaqiang, G. Maochu, C. Yaoqiang, Appl. Surf. Sci. 273 (2013) 527.
[9] J. Fan, X. Wu, Q. Liang, R. Ran, D. Weng, Appl. Catal. B: Environ. 81 (2008) 38.
[10] R. Si, Y.-W. Zhang, L.-M. Wang, S.-J. Li, B.-X. Lin, W.-S. Chu, Z.-Y. Wu, C.-H. Yan, J. Phys. Chem. C 111 (2006) 787.
[11] G.L. Markaryan, L.N. Ikryannikova, G.P. Muravieva, A.O. Turakulova, B.G. Kostyuk, E.V. Lunina, V.V. Lunin, E. Zhilinskaya, A. Aboukais, Colloids Surf. A: Physicochem. Eng. Aspects 151 (1999) 435.
[12] H. He, H.X. Dai, L.H. Ng, K.W. Wong, C.T. Au, J. Catal. 206 (2002) 1.
[13] C.K. Narula, L.P. Haack, W. Chun, H.W. Jen, G.W. Graham, J. Phys. Chem. B 103 (1999) 3634.
[14] R. Ran, D. Weng, X. Wu, J. Fan, L. Wang, X. Wu, J. Rare Earths 29 (2011) 1053.
[15] J. Mikulova, S. Rossignol, F. Gérard, D. Mesnard, C. Kappenstein, D. Duprez, J. Solid State Chem. 179 (2006) 2511.
[16] A. Bortun, J. Nunan, Niobium containing zirconium-cerium based solid solutions, US 6,605,264 B2 Delphi Technologies (2003).
[17] L.F. Liotta, A. Macaluso, A. Longo, G. Pantaleo, A. Martorana, G. Deganello, Appl. Catal. A: Gen. 240 (2003) 295.
[18] A.I. Kozlov, D.H. Kim, A. Yezerets, P. Andersen, H.H. Kung, M.C. Kung, J. Catal. 209 (2002) 417.
[19] R. Wang, P.A. Crozier, R. Sharma, J. Mater. Chem. 20 (2010) 7497.
[20] H. Vidal, J. Kašpar, M. Pijolat, G. Colon, S. Bernal, A. Cordón, V. Perrichon, F. Fally, Appl. Catal. B: Environ. 30 (2001) 75.
[21] X. Wu, X. Wu, Q. Liang, J. Fan, D. Weng, Z. Xie, S. Wei, Solid State Sci. 9 (2007) 636.
[22] D.-J. Kim, H.-J. Jung, I.-S. Yang, J. Am. Ceram. Soc. 76 (1993) 2106.
[23] D.Y. Lee, J.-W. Jang, D.-J. Kim, Ceram. Int. 27 (2001) 291.